

Supporting information

Chiral Se@CeO₂ Superparticles for Ameliorating Parkinson's Disease

Ximing Liu^{1,2}, Hongyu Zhang^{1,2}, Changlong Hao^{1,2*}, Hua Kuang^{1,2}, Chuanlai Xu^{1,2*}, Liguang Xu^{1,2*}

¹International Joint Research Laboratory for Biointerface and Biodetection, Jiangnan University, Wuxi, Jiangsu, 214122, PRC; ²State Key Laboratory of Food Science and Technology, Jiangnan University, JiangSu, PRC.

Email: hcl@jiangnan.edu.cn; xlq@jiangnan.edu.cn

EXPERIMENTAL SECTION

Chemicals and reagents. Cerium nitrate hexahydrate (CeN₃O₉·6H₂O, 99.5% metals basis), selenium dioxide (SeO₂, 99.9% metals basis), polyvinylpyrrolidone (PVP, 99%), D-CYS (99%), L-CYS (99%), DL-CYS (99%), phospholipid-PEG-amino, 3,3',5,5'-tetramethylbenzidine (TMB), terephthalic acid (TA), and ethanol were all purchased from Sigma-Aldrich (St. Louis, Missouri, USA). All aqueous solutions in the experiment were prepared using ultrapure water (≥ 18.25 MΩ, Milli-Q, Millipore). The Superoxide Dismutase (SOD), Glutathione Peroxidase (CAT), and Catalase (CAT) Assay Kits, were purchased from Beyotime Biotechnology (Shanghai, China). The ELISA kit for α-synuclein detection was obtained from JingKang Bio. Antibodies for ionized calcium-binding adapter molecule 1 (IBA-1), tyrosine hydroxylase (TH), caspase-3, and β-actin, along with the appropriate fluorescent secondary antibodies, were purchased from Thermo Fisher Co., Ltd. (Scotts Valley, CA, USA). All chemicals and reagents were used as received without any further purification.

Instruments. Transmission electron microscopy (TEM) images were obtained

with a JEOL, JEM-2100 transmission electron microscope operated at 200 kV. X-ray diffraction (XRD) patterns were acquired on a Bruker D8 Advanced X-ray powder diffractometer with Cu-K α radiation at 40 kV ($\lambda=1.5418 \text{ \AA}$). The composition of materials was verified by an X-ray photoelectron spectral system (XPS, Kratos Analytical Axis Ultra). Confocal images were obtained using a Leica LSM880 confocal fluorescence microscope (Leica Microsystems, Wetzlar, Germany). The CD signals were characterized by a CHIRASCAN CD spectrometer from Applied Photophysics (Surrey, UK) with an optical path length of 1 cm.

Synthesis of chiral Se nanoparticles. In brief, 1 mL of ultrapure water, 0.05 mL of 1% (wt%) PVP solution and 0.5 mL of 0.1 M SeO₂ solution were added to a round-bottomed flask and stirred until dissolved. Then, 0.5 mL of 0.3 M of *L*-, *D*-, and *DL*-Cys were added with vigorous stirring. The mixture was allowed to react at room temperature. After 10 min, 0.5 mL of 0.3 M NaBH₄ was added. The mixture was stirred overnight at room temperature under an N₂ atmosphere to create the final products. The chiral Se NPs were centrifuged at 5,000 r/min for 10 min. The precipitate was collected and suspended in water.

Synthesis of CeO₂ nanoparticles. In brief, 1 mL of Milli-Q water and 0.05 mL of 1% PVP solution were added to a round-bottomed flask and stirred until dissolved. Then, 0.5 mL of 0.3 M peptide *L*, *D*, and *DL*-Cys and 0.5 mL of 0.1 M Ce(NO₃)₃·6H₂O were added with vigorous stirring. The mixture was allowed to react at room temperature. After 10 min, 0.5 mL of 0.3 M NaBH₄ was added. The mixture was stirred overnight at room temperature under an N₂ atmosphere to create the final products. The

CeO₂ NPs were centrifuged at 6,500 r/min for 10 min. The precipitate was collected and suspended in water.

Synthesis of Se@CeO₂ superparticles. In brief, 1 mL of Milli-Q water, 0.05 mL of 1% PVP solution and 0.5 mL of 0.1 M SeO₂ solution were added to a round-bottomed flask and stirred until dissolved. Then, 0.5 mL of 0.3 M peptide *L, D, DL*-Cys and 0.5 mL of 0.1 M Ce(NO₃)₃·6H₂O were added with vigorous stirring. The mixture was allowed to react at room temperature. After 10 min, 0.5 mL of 0.3 M NaBH₄ was added. The mixture was stirred overnight at room temperature under an N₂ atmosphere to create the final products. The Se@CeO₂ SPs were centrifuged at 4,500 r/min for 10 min. The precipitate was collected and suspended in water. Then the solution was centrifuged at 4,500 r/min for 10 min. After three-time centrifugation, the purified Se@CeO₂ SPs were collected and stored in refrigerator.

Superoxide dismutase (SOD)-like activity of Se@CeO₂ superparticles. The SOD-like activity of Se@CeO₂ SPs, and comparisons with the SOD enzyme, were determined by the Total Superoxide Dismutase Assay Kit with 2-(2-methoxy-4-nitrophenyl)-3-(4-nitrophenyl)-5-(2,4-disulfophenyl)-2H-tetrazolium (WST-8), following the manufacturer's guidelines. Water-soluble formazan dye was then generated by the reaction of WST-8 with ·O₂⁻, which was generated by xanthine oxidase (XO). In the presence of SOD enzyme, the amount of ·O₂⁻ decreased along with an increase in the absorbance of formazan dye at 450 nm.

Catalase (CAT)-like activity of Se@CeO₂ superparticles. The CAT-like activity of Se@CeO₂ SPs was determined by a Catalase Assay Kit. In the presence of

sufficient H_2O_2 and a limited amount of CAT enzyme, the resultant red solution, which showed absorbance at 540 nm, was oxidized by the remaining H_2O_2 in the presence of POD. The CAT-like activity of Se@CeO_2 SPs was also examined by fluorescence spectroscopy. Terephthalic acid (TA) can react with $\cdot\text{OH}$ and generate fluorescent 2-hydroxyterephthalic acid (TA-2-OH). However, in the presence of CAT, H_2O_2 decomposed into H_2O and O_2 instead of $\cdot\text{OH}$. Therefore, the fluorescence signal of TA-2-OH reflected the activity of the enzyme. 10 mM H_2O_2 diluted in PBS was mixed with Se@CeO_2 SPs (20 $\mu\text{g}/\text{mL}$) with vigorous stirring and incubated at room temperature for 6 h. Then, 5 mM TA in DMF was added to the solution and the fluorescence spectrum was recorded with excitation at 320 nm.

Glutathione peroxidase (GPx)-like activity of Se@CeO_2 superparticles. GPx-like activity was determined by the Glutathione Peroxidase Assay Kit with NADPH in accordance with the manufacturer's instructions. In brief, GSSG was generated by the reaction of GPx with GSH. In the presence of glutathione reductase, NADPH could react with GSSH and produce GSH. Therefore, a reduction in NADPH reflected the activity of GPx and could be determined by the absorbance at 340 nm. Experimental conditions: GR (1.7 units), GSH (2 mM), NADPH (2 mM), *L*-SP (20 $\mu\text{g}/\text{mL}$) and Se+CeO_2 (20 $\mu\text{g}/\text{mL}$) in PBS (10 mM, pH=7.4) at 25 °C.

Peroxidase (POD)-like activity of Se@CeO_2 superparticles. The POD-like activity of Se@CeO_2 SPs was determined using TMB as a substrate. In the presence of POD, TMB can react with H_2O_2 and generate a yellow product with a pH<1. To detect the enzyme-like activity of Se@CeO_2 SPs, 0.5 mM of TMB, 20 $\mu\text{g}/\text{mL}$ of Se@CeO_2

SPs and H₂O₂ were mixed together at different concentrations. After sufficient mixing, H₂SO₄ was added to adjust the pH and the absorbance of the mixture was detected at 450 nm to evaluate POD-like activity.

Steady-state kinetic assays. Steady-state kinetic assays were performed at room temperature. All the reactions were monitored by measurement of the absorbance at different reaction times. The catalytic parameters were determined by fitting the absorbance data to the Michaelis-Menten equation, which describes the relationship between the rate of substrate conversion by an enzyme (Se@CeO₂ SPs) and the concentration of the substrate, as shown in the following equation:

$$V = \frac{V_{\max}[S]}{K_m + [S]}$$

In this equation, v is the rate of conversion, V_{\max} is the maximum rate of conversion, $[S]$ is the concentration of substrate, and K_m is the Michaelis constant. K_m is equivalent to the substrate concentration at which the rate of conversion is half of V_{\max} . K_m indicates the affinity of the enzyme for the substrate: a low K_m value represents high affinity.

Evaluation of the hydroxyl radical (\cdot OH) scavenging activity. A fluorescence method was also used to evaluate the \cdot OH-scavenging activity. Briefly, \cdot OH was produced by the Fenton reaction between 2 mM FeSO₄ and 5 mM H₂O₂ for 10 min. The amount of \cdot OH scavenged was detected by measuring the characteristic absorbance of 2,3-dihydroxy-benzoic acid at 510 nm, which was produced from the reaction of salicylic acid (1.5 mM) with \cdot OH.

Cell culture. All cells were cultured at 37°C in a humidified atmosphere of 5% CO₂ and 95% air. MN9D cells were grown in DMEM medium supplemented with 10% FBS and 1% penicillin/streptomycin.

Cellular toxicity. MN9D cells were placed in 96-well plates and incubated for 24 h. Then, new culture medium, containing different concentrations of Se@CeO₂ SPs, was added to replace the old medium. After 24 h incubation, cell viability was assessed using the standard Cell Counting Kit-8 (CCK-8) in accordance with the manufacturer's instructions.

Intracellular reactive oxygen species (ROS) detection. The oxidant-sensitive fluorescent dye 2',7'-dichlorodihydrofluorescein diacetate (DCFH-DA) was used to determine the intracellular ROS level (Reactive Oxygen Species Assay Kit, Beyotime Institute of Biotechnology, China). Pretreated cells were incubated with new culture medium containing 10 μM DCFH-DA at 37°C for 30 min. The cells were then washed with PBS three times to remove the excess dye. After that, the fluorescence intensity of each well was measured with an excitation wavelength of 488 nm. The emission peak was monitored at 525 nm. The ROS level was expressed as the ratio of $(F_{\text{test}} - F_{\text{blank}})/(F_{\text{control}} - F_{\text{blank}})$, where F_{test} is the fluorescence intensity of the pretreated cells, F_{blank} is the fluorescence intensity of the wells without cells, and F_{control} is the fluorescence intensity of the untreated cells.

Levels of caspase-3 in vitro. Cells were fixed with 4% paraformaldehyde for 15 min, permeabilized with 0.1% Triton X-100 for 2 min and blocked with 1% bovine serum albumin (BSA) for 2 h at room temperature. Then, incubation with anti-cleaved

caspase-3 was maintained at room temperature for 2 h. Subsequently, the cells were washed with PBS and then incubated with Alex488-conjugated (goat-anti-rabbit) secondary antibody (1:500) at room temperature for 2 h. After washing with PBS, the cells were captured using a Leica LSM880 confocal fluorescence microscope. Western blotting was also used to characterize the effects of Se@CeO₂ SPs to reduce the level of caspase-3 in MN9D cells.

Flow cytometry assays. Flow cytometry was used to detect the proportion of apoptotic cells. MN9D cells (1.0×10^6) undergoing different treatments with MPP⁺ and Se@CeO₂ SPs were collected by centrifugation. The detection of apoptosis in MN9D cells was carried out with an Annexin V-FITC Apoptosis detection kit, in accordance with the manufacturer's instructions.

Cell survival assay for chiral Se@CeO₂ superparticles. MN9D cells were plated in 96-well plates and incubated for 24 h. Then, new culture medium containing different concentrations of Se@CeO₂ SPs was added to replace the old medium. After 12 h incubation, different concentrations of MPP⁺ were added to the medium, and the cells were incubated for another 12 h. Then, cell viability was assessed using the standard CCK-8 kit according the manufacturer's instructions.

Different cellular internalization patterns of the Se@CeO₂ SPs. MN9D cells were incubated with Se@CeO₂ SPs at the same concentration for 24 h. The cells were then used to obtain confocal images of the time-dependent concentration of Se@CeO₂ SPs, within the cells. MN9D cells incubated at 4°C or with CPZ (chlorpromazine) or M β -CD (methyl β -cyclodextrin) for 12 h, were fixed with 4% paraformaldehyde for 15

min, permeabilized with 1% Triton X-100 for 2 min, and blocked with 1% bovine serum albumin (BSA) for 2 h at room temperature. After washing with PBS, the cells were imaged using a Leica LSM880 confocal fluorescence microscope.

***In vivo* therapeutic effects of chiral Se@CeO₂ superparticles in the animal model.** In this study, PD model mice were given 1-methyl-4-phenyl-1,2,3,6-tetrahydropyridine (MPTP). We used 8–10-week-old male C57BL/6 mice. MPTP was dissolved in saline and administered by subcutaneous injection with 30 mg kg/d MPTP for 8 d and the control mice were given saline once daily for 8 d. All animal treatment and maintenance protocols were approved by the Institutional Animal Care and Use Committee of Jiangnan University.

Stereotaxic injection. After anesthetization with isoflurane, the C57BL/6 mice were placed in a stereotaxic frame. Saline or Se@CeO₂ SPs solution (0.2 mg/mL, 4 μL) was injected into the striatum through the apparatus for 15 days.

Immunohistochemistry and immunohistofluorescence. Tyrosine hydroxylase (TH) immunohistochemistry was used to evaluate dopaminergic neuronal degeneration. The mice were anesthetized with isoflurane, and perfused with 4% paraformaldehyde in PBS. Their brains were removed and fixed with 4% paraformaldehyde in 0.1 M phosphate buffer at 4°C for 20 h, incubated in 30% sucrose in 0.05 M PBS for 72 h, and cut into 30 μm sections using a cryostat. The tissue sections were incubated at 4°C overnight with anti-TH antibody (1:1000; Abcam ab112) or anti-IBA1 antibody (1:1000; Thermo Fisher, PA5-27436). Horseradish-peroxidase-conjugated anti-rabbit IgG antibody (1:500; Abcam ab205718) and Alexa-Fluor-647-conjugated anti-rabbit

IgG antibody (1:500; Thermo Fisher A-21245) were used as the secondary antibodies for immunohistochemistry and immunohistofluorescence, respectively.

Morris water maze task. The maze consisted of a circular pool of blue opaque plastic, with a depth of 50 cm and a width of 120 cm. The water was maintained at 24–26°C with an automatic heater to avoid hypothermia. On the first five consecutive days, the mice (n = 8 per group) performed three acquisition trials daily, with a 15 min intertrial interval. Briefly, three starting points, excluding the only quadrant without a platform, were randomly selected in the three daily trials. Each mouse, while facing the wall of the tank, was set free into the water. If the mouse failed to reach the platform within 90 s, it was guided to the platform and remained there for 30 s. Within the intertrial intervals, the mice were towel dried in a plastic holding cage filled with additional towels. Upon completion of the three daily trials, the mice were removed from the maze, towel dried, and returned to the home cage. Finally, on the sixth day, a spatial memory test was performed by each mouse through a probe trial. Briefly, the fixed platform was removed from the maze, and each mouse was released into the water at a position right opposite the escape platform and allowed to swim freely for 60 s. Spatial acuity was expressed as the percentage of time the mouse spent in the southeast quadrant where the escape platform was located.

Histological examination. Se@CeO₂ (0.2 mg/mL, 200 µL) was injected via the tail vein in mice for 15 days. The mice were killed and their major organs collected, including the heart, liver, spleen, lung, and kidney. Each sample was stained with H&E,

and then examined with fluorescence microscopy to investigate the biocompatibility of the Se@CeO₂ SPs in these tissues.

Biochemical assay. Blood samples were collected via the ocular vein. Serum was obtained by centrifuging whole blood at 5000 g for 10 min. Liver function was evaluated by serum levels of alkaline phosphatase, alanine aminotransferase, and aspartate aminotransferase. Nephrotoxicity was measured by the blood urea nitrogen level. These biochemical parameters were determined with an automated biochemical analyzer.

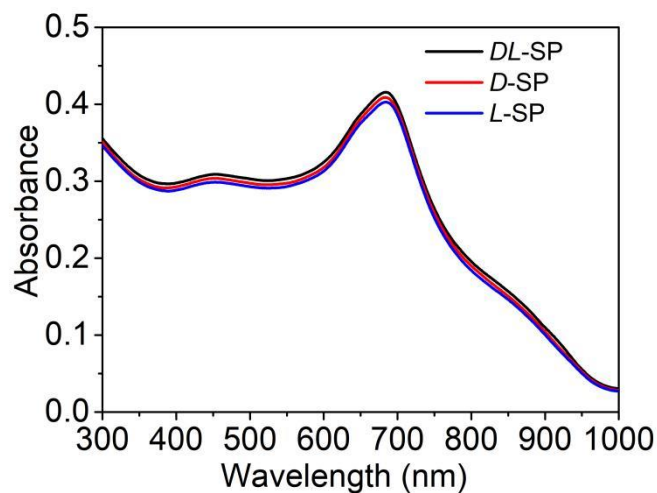


Figure S1. UV-vis spectra of the *D*-, *L*-, and *DL*-SP.

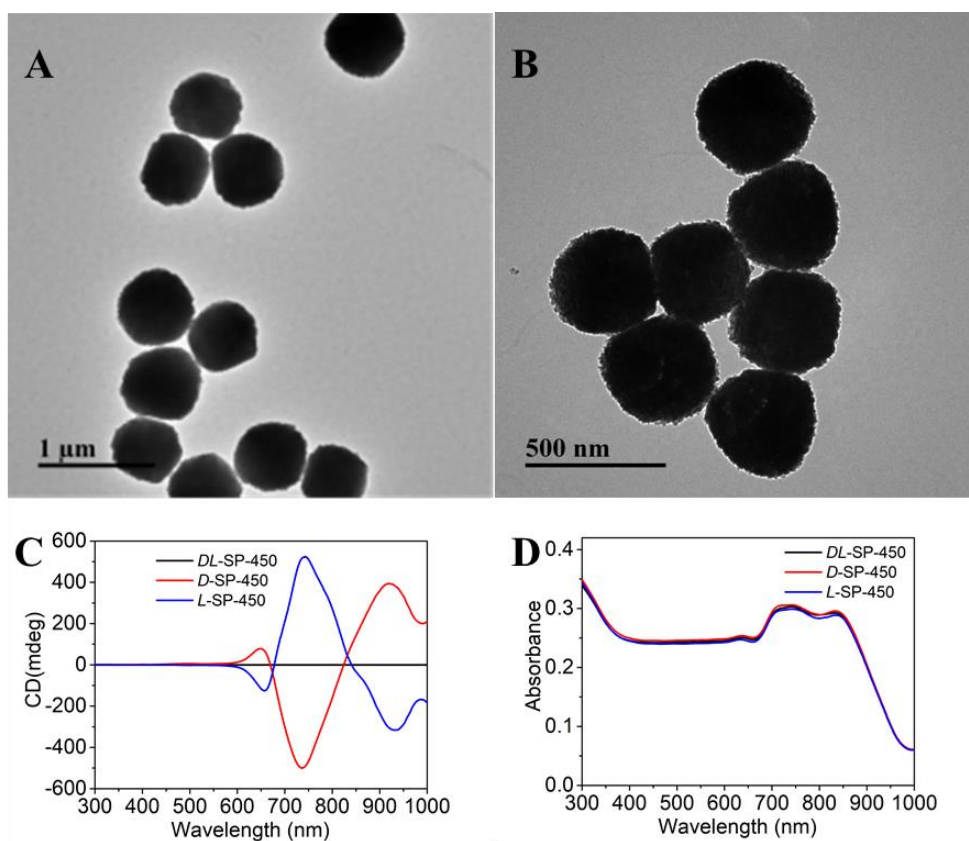


Figure S2. (A) TEM image of the *L*-SP-450. (B) TEM image of the 450nm *D*-SP-450. (C, D) CD and UV-vis spectra of the *DL*-, *D*-, *L*-SP-450.

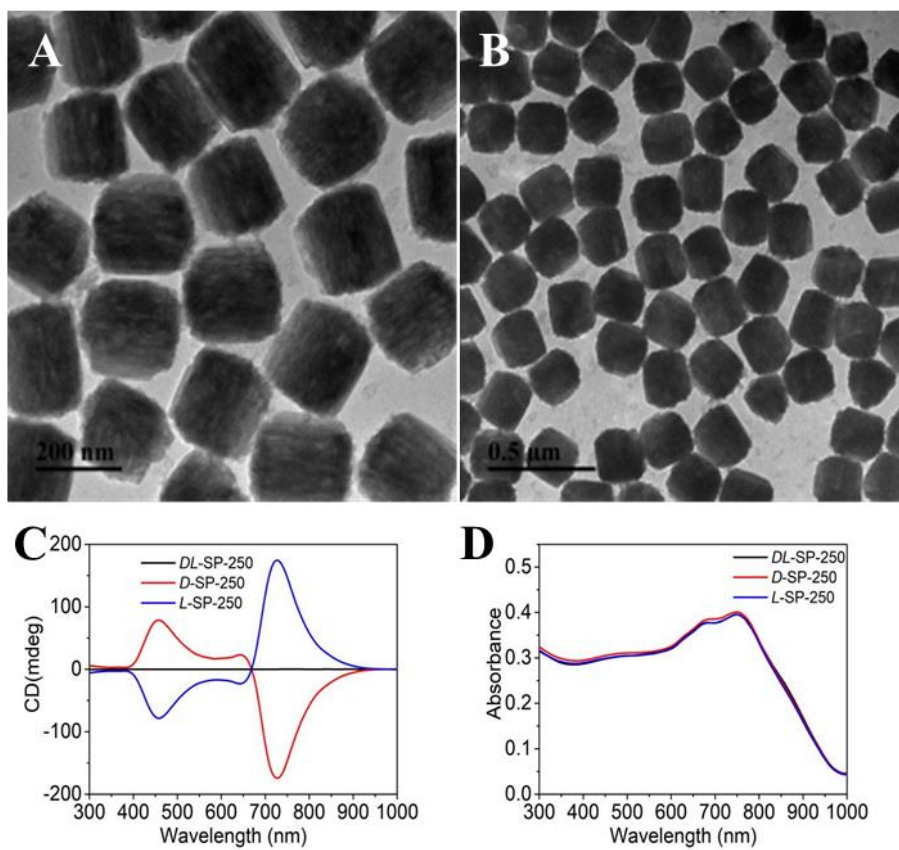


Figure S3. (A) TEM image of the *L*-SP-250. (B) TEM image of the 250nm *D*-SP-250. (C, D) CD and UV-vis spectra of the *DL*-, *D*-, *L*-SP-250.

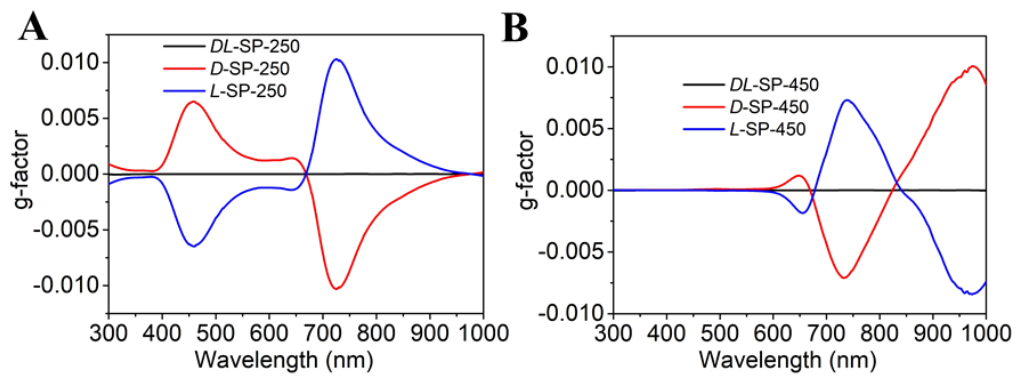


Figure S4. (A) g-factor of the *D*-, *L*-, and *DL*-SP-250. (B) g-factor of the *D*-, *L*-, and *DL*-SP-450.

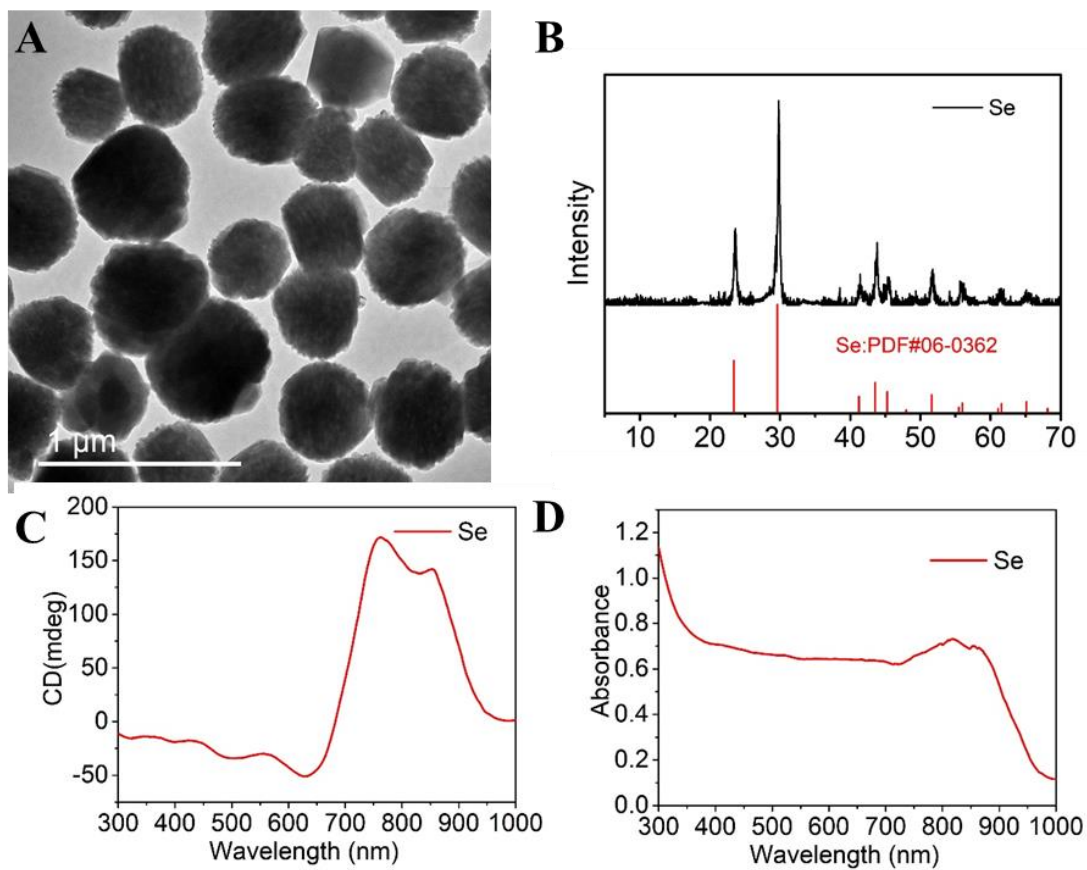


Figure S5. (A) TEM image of the Se NP. (B) Powder X-ray diffraction (XRD) patterns of the Se NP. (C, D) CD and UV-vis spectra of the Se NP.

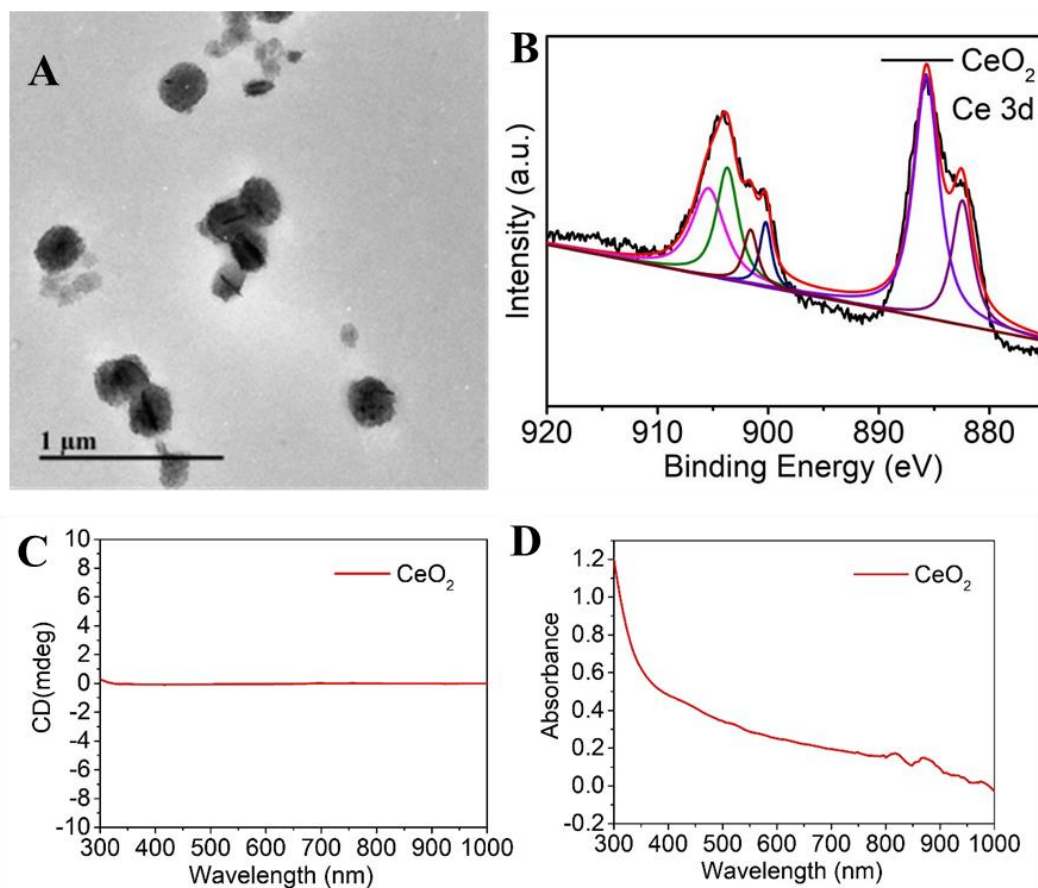


Figure S6. (A) TEM image of the CeO₂ NP. (B) XPS spectra of the CeO₂ NP, fitted Ce 3d photoelectron peaks.

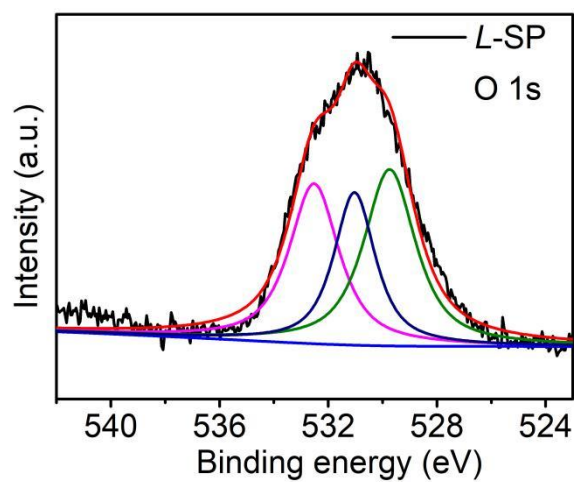


Figure S7. XPS data of the *L*-SP, fitted O 1s photoelectron peaks.

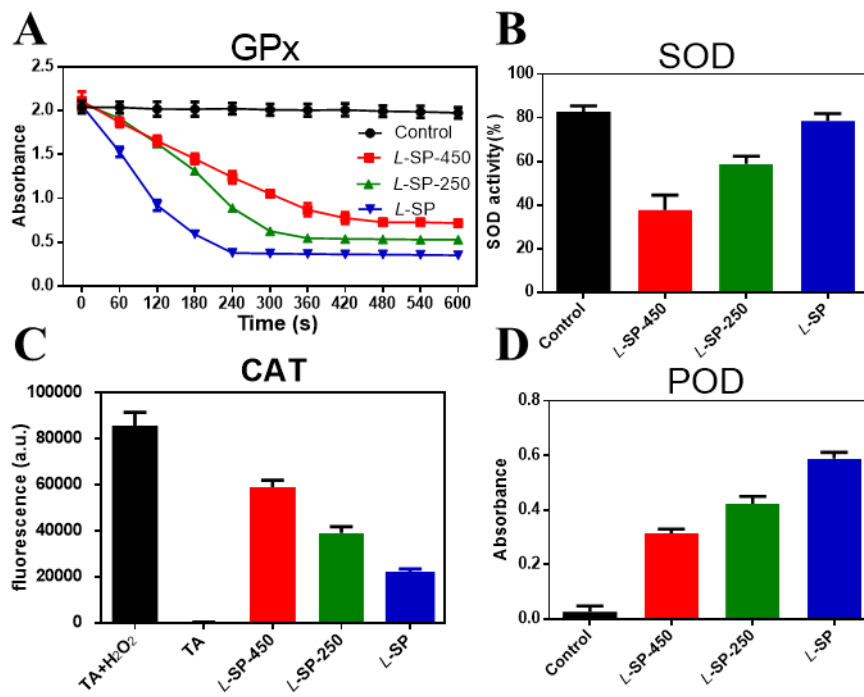


Figure S8. Comparison of GPx, SOD, CAT, and POD-like activity of *L*-SP-450, *L*-SP-250 nm, *L*-SP.

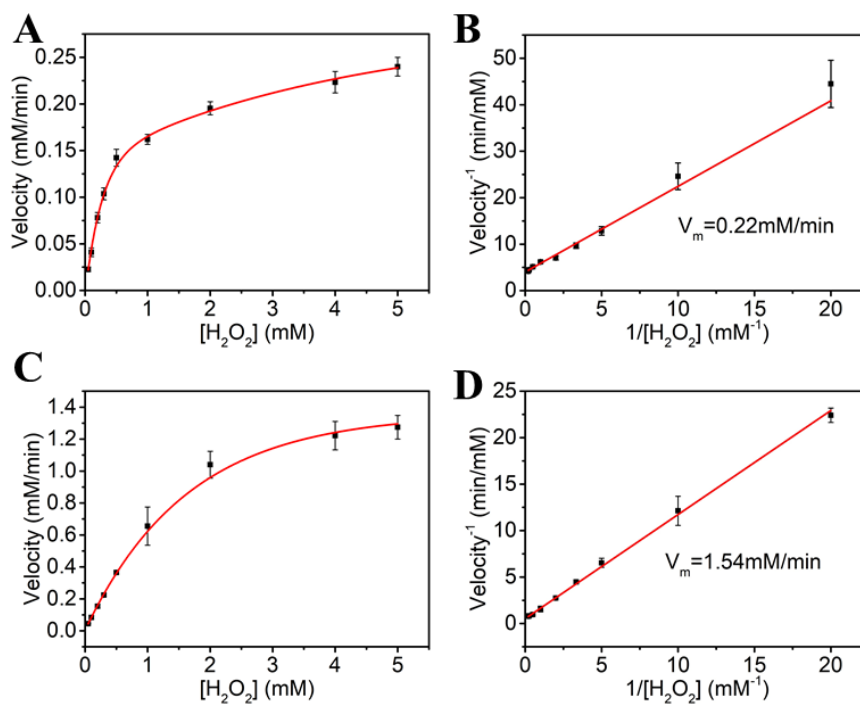


Figure S9. The CAT-like activity of Se+CeO₂ and L-SP. Steady-state kinetic assay of Se+CeO₂ (A-B) and L-SP (C-D) with H₂O₂. (A, C) Michaelis-Menten plot and (B, D) corresponding Lineweaver-Burk plot of the CAT-like activity of the Se+CeO₂ and L-SP in PBS (10 mM, pH 7.4) at 25 °C.

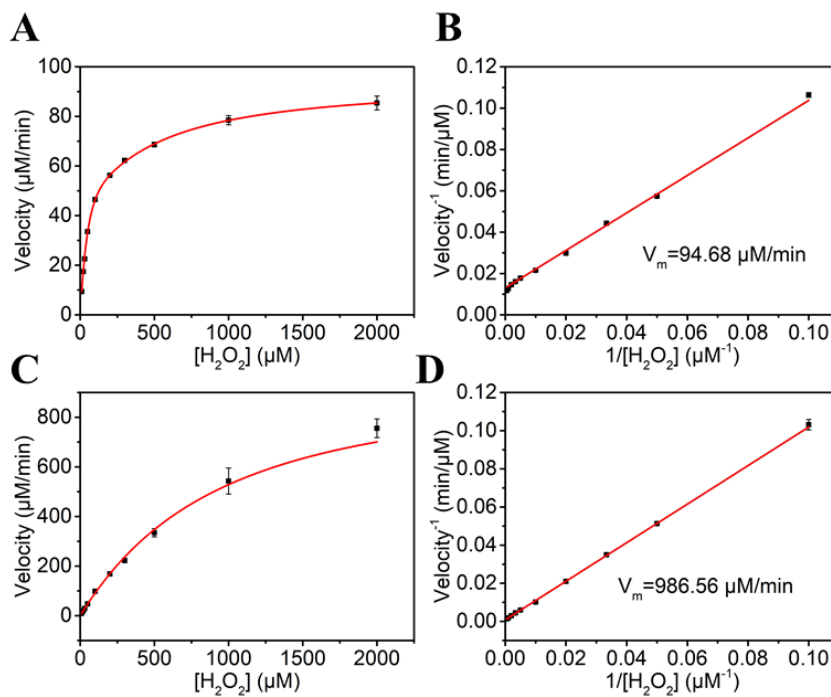


Figure S10. The GPx-like activity of Se+CeO₂ and L-SP. Steady-state kinetic assay of Se+CeO₂ (A-B) and L-SP (C-D) with H₂O₂. (A, C) Michaelis-Menten plot and (B, D) corresponding Lineweaver-Burk plot of the GPx-like activity of the Se+CeO₂ and L-SP in PBS (10 mM, pH 7.4) at 25 °C. Experimental conditions: GR (1.7 units), GSH (2 mM), NADPH (2 mM), L-SP and Se+CeO₂ in PBS (10 mM, pH=7.4) at 25 °C.

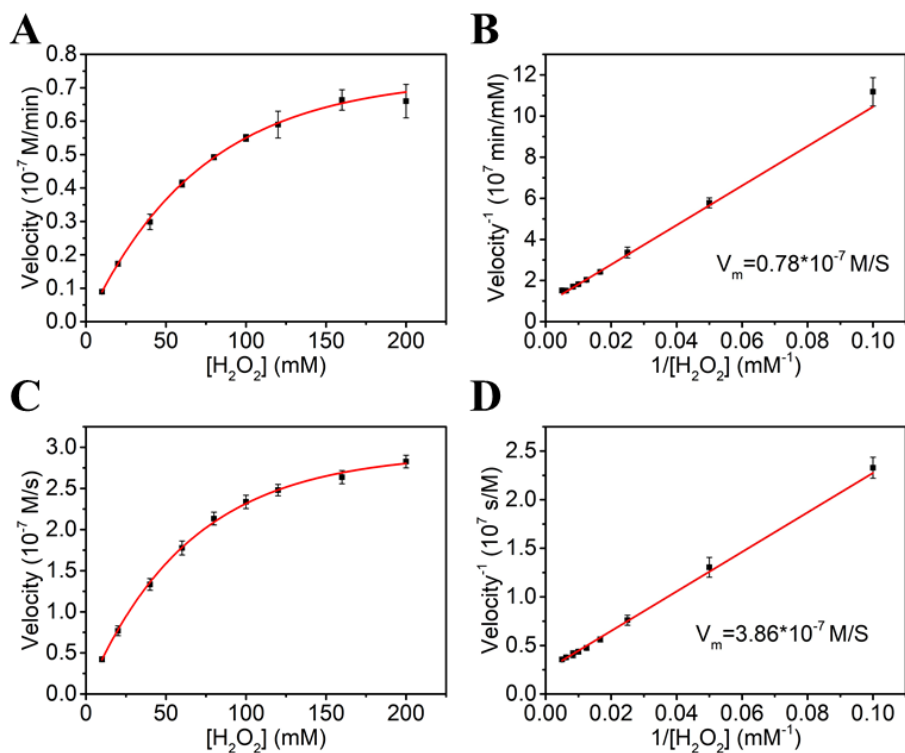


Figure S11. The POD-like activity of Se+CeO₂ and L-SPs. Steady-state kinetic assay of Se+CeO₂ (A-B) and L-SP (C-D) with H₂O₂. (A, C) Michaelis-Menten plot and (B, D) corresponding Lineweaver-Burk plot of the POD-like activity of the Se+CeO₂ and L-SP. The steady-state catalytic rate was calculated from the initial slope of the absorbance vs. time curves. The absorbance data were used to back-calculate the concentration by the Beer–Lambert Law using a molar absorption coefficient of 39,000 M⁻¹ cm⁻¹ for the oxidation products of TMB.

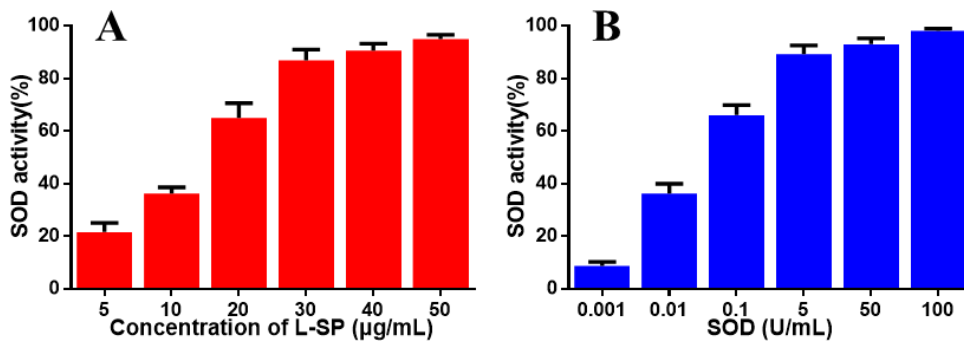


Figure S12. The SOD-like activity of the *L*-SP. Comparative analysis of the $O_2^{\bullet-}$ -scavenging ability of the *L*-SP with that of the SOD enzyme (1000U/mg). (A) SOD-like activity of the *L*-SP (5-50 μ g/mL). (B) Activity of the natural SOD enzyme (10^{-3} -100 U/mL).

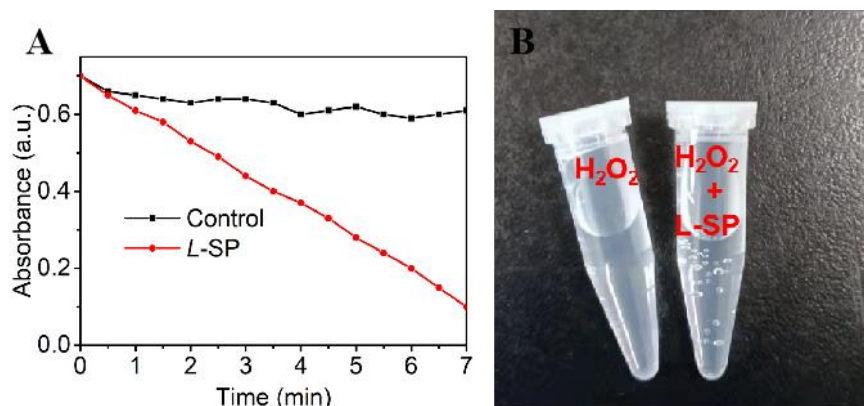


Figure S13. The CAT-like activity of the *L*-SP. (A) Plot of the absorbance versus time for the reaction of H_2O_2 (2 mM) in the presence of the *L*-SP (10 μ g/mL). H_2O_2 (2 mM) alone in the absence of the *L*-SP was used as the control. (B) The formation of bubbles reveals the decomposition of H_2O_2 by the *L*-SP.

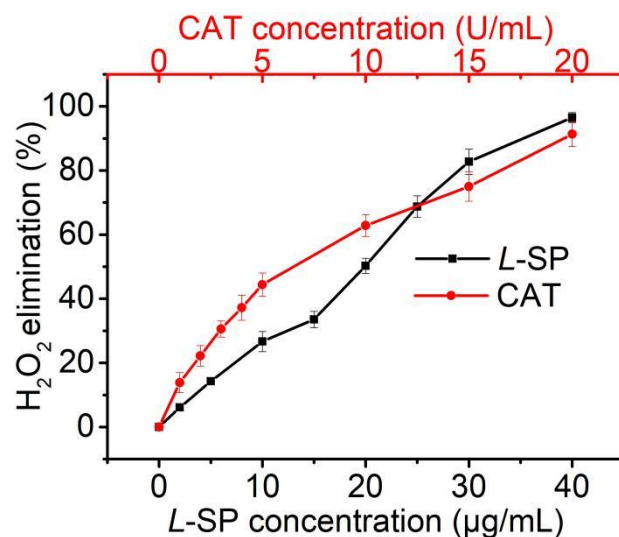


Figure S14. The CAT-like activity of the *L*-SP. Dependence of H₂O₂ elimination on the concentration of the *L*-SP (0-40 µg/mL) or natural CAT enzyme (0-20 U/mL, 3000U/mg).

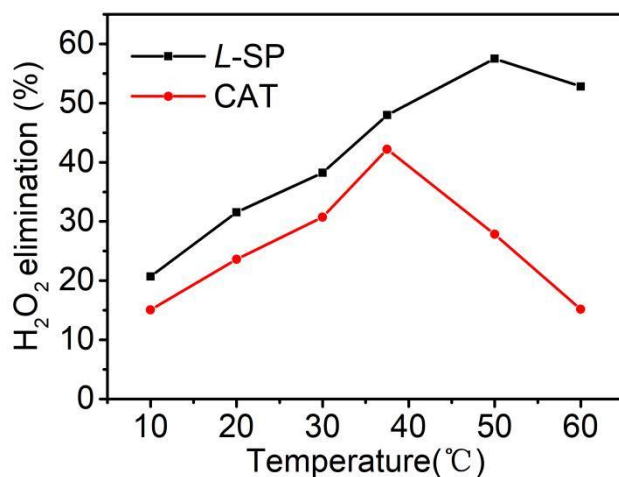


Figure S15. The CAT-like activity of the *L*-SP. H₂O₂ elimination efficiencies of the *L*-SP (20 µg/mL) and natural CAT (10 U/mL) pretreated at different temperatures. The concentration of H₂O₂ was fixed at 2 mM.

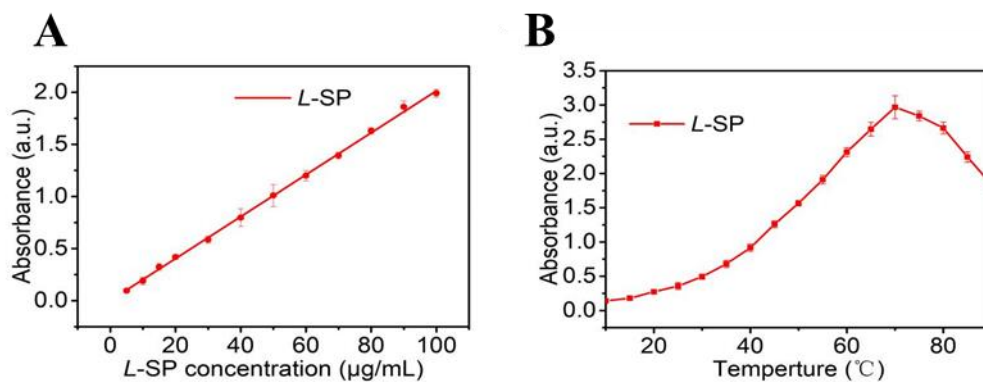


Figure S16. The POD-like activity of the *L*-SP. Temperature and concentration dependence of the POD-like activity of the *L*-SP. (A) The absorbance associated with different concentrations of the *L*-SP (5-100 µg/mL) in the reaction system after 2 min. (B) The absorbance changes with the increase in temperature from 10 °C to 90 °C.

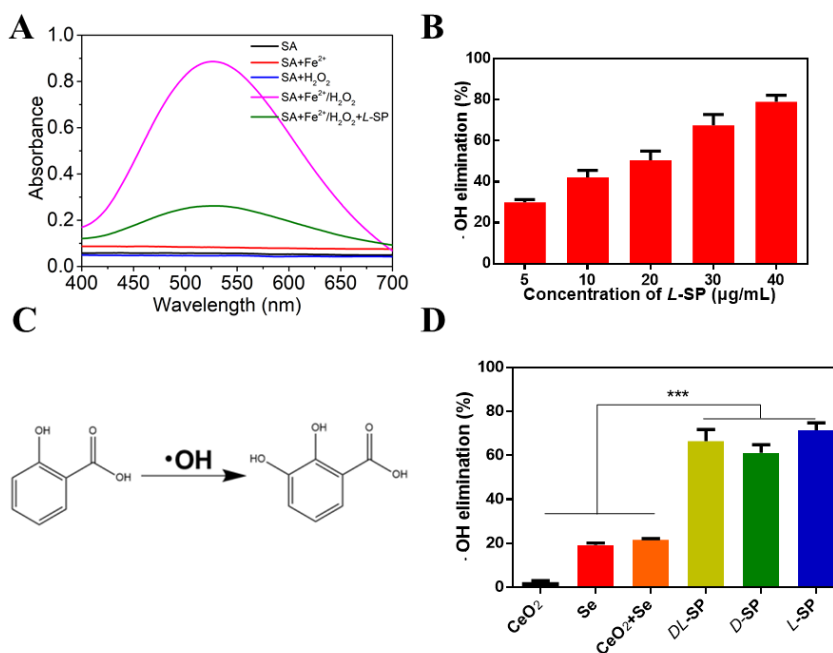


Figure S17. •OH-scavenging activity of the *L*-SP. (A) Absorption spectra of salicylic acid (SA) after reaction with FeSO₄/H₂O₂, in the absence and presence of the SP. SA alone, and SA reacted with FeSO₄ or H₂O₂ were used as control. (B) Dependence of •OH elimination on the concentration of the *L*-SP. (C) Reaction mechanism of Fenton reaction. (D) Comparison of •OH-scavenging activity of CeO₂ NP, Se NP, CeO₂+Se, *DL*-SP, *D*-SP, *L*-SP, *** *P* (t-test) < 0.001 with reference to Control.

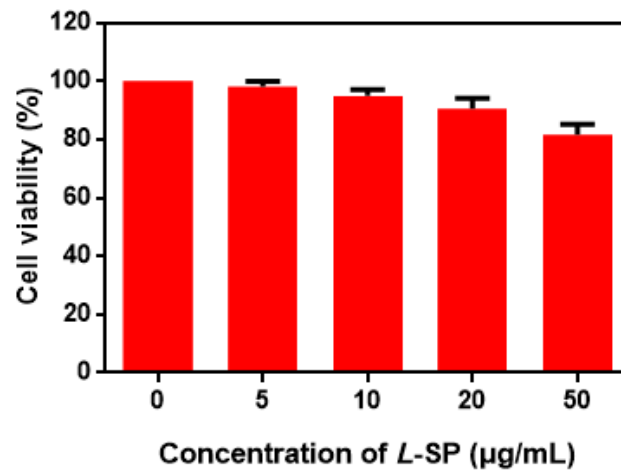


Figure S18. MN9D cell viability under different concentrations of the *L*-SP.

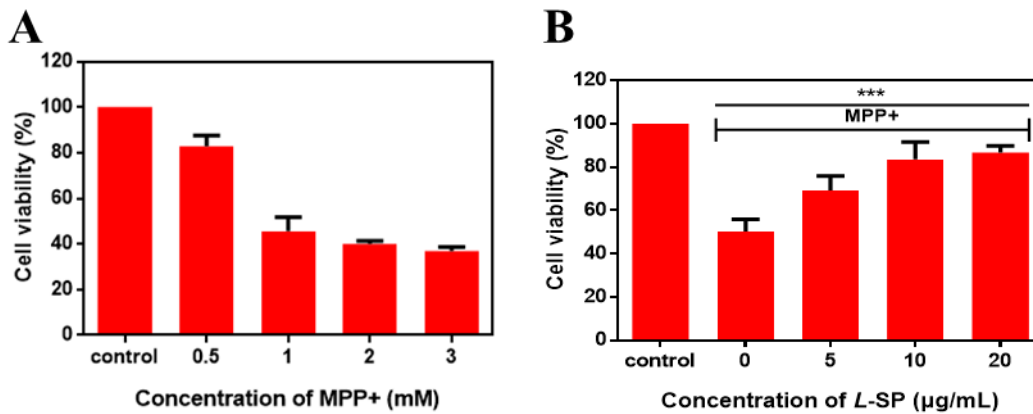


Figure S19. (A) Viability of MN9D cells incubated with different concentrations of MPP+. (B) Cell viability measurements of MPP+ treated MN9D cells in the presence of different the *L*-SP concentrations. The concentration of MPP+ was set at 1 mM. All the data is represented as mean \pm SD, $n=5$, *** P (t-test) < 0.001 with reference to Control.

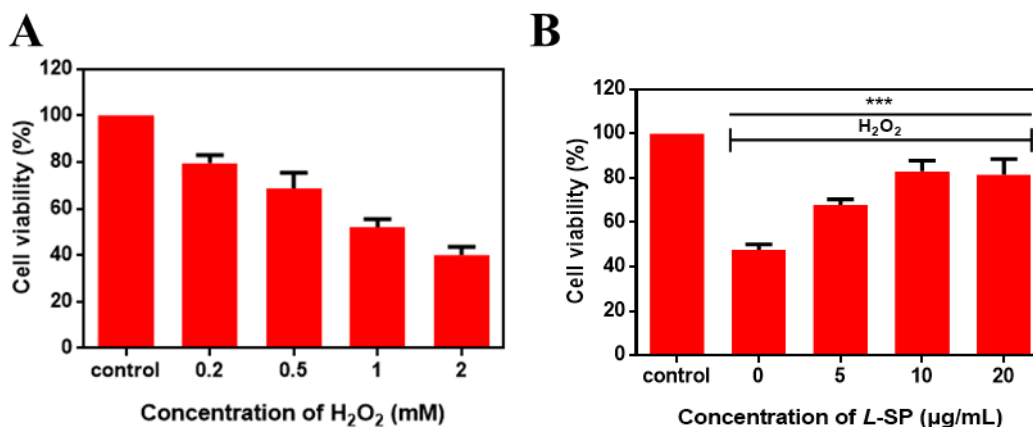


Figure S20. (A) Viability of MN9D cells incubated with different concentrations of H₂O₂. (B) Cell viability measurements of H₂O₂ treated MN9D cells in the presence of different the L-SP concentrations. The concentration of H₂O₂ was set at 1 mM. All the data is represented as mean \pm SD, $n=5$, *** P (t-test) < 0.001 with reference to Control.

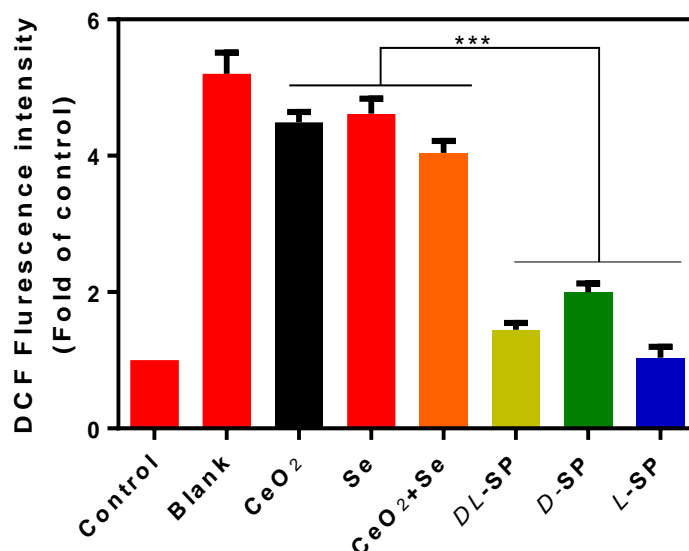


Figure S21. The intracellular ROS level in the presence of MPP⁺ with different treatments was expressed by the ratio of $(F_{\text{test}} - F_{\text{blank}}) / (F_{\text{control}} - F_{\text{blank}})$, where F_{test} is the fluorescence intensity of pretreated cells, F_{blank} is the fluorescence intensity of PBS, and F_{control} is the fluorescence intensity of untreated cells. Data are presented as mean \pm s. d. ($n = 5$), *** P (t-test) < 0.001 with reference to Control.

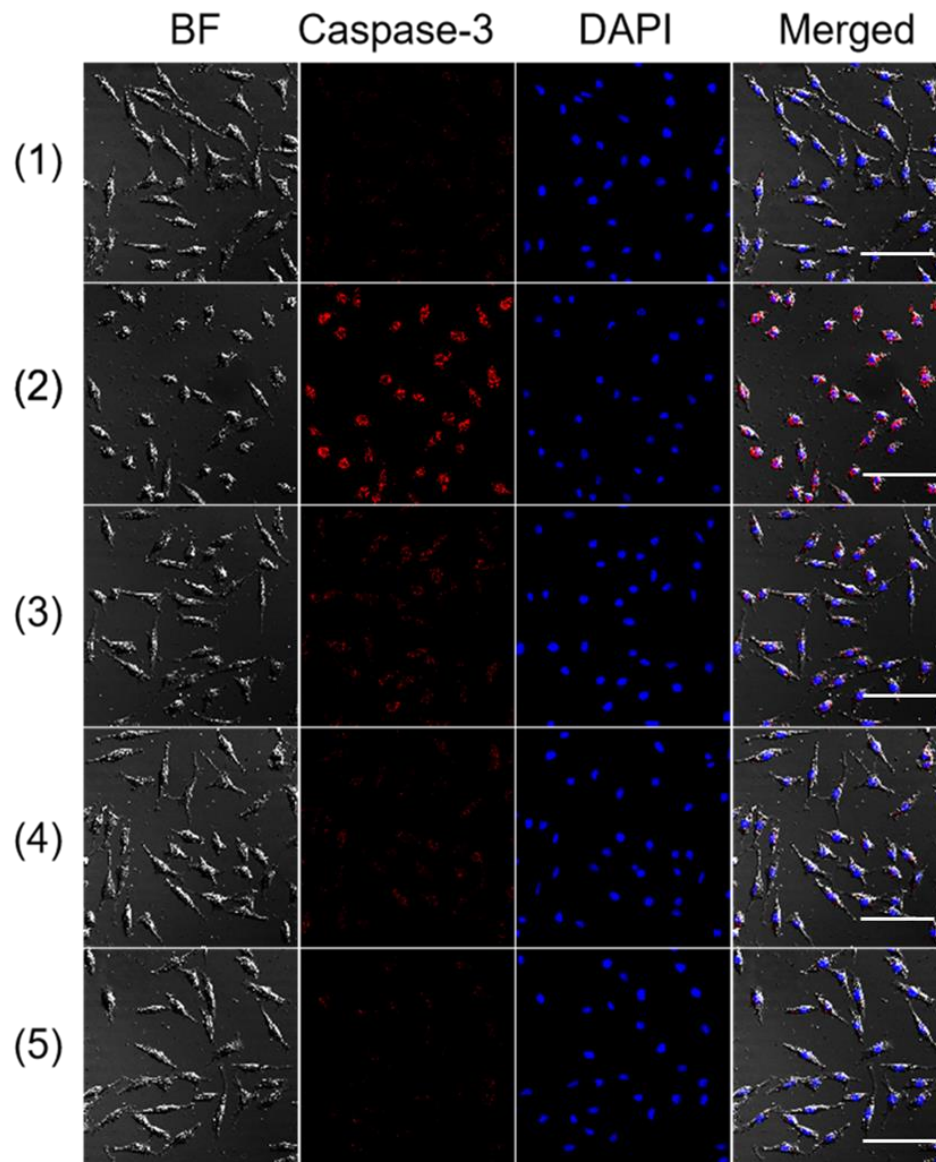


Figure S22. Confocal images of MN9D cells with different treatments: (1) control and (2) 1 mM H₂O₂, (3) 1 mM H₂O₂ and 5 μg/mL *L*-SP, (4) 1 mM H₂O₂ and 10 μg/mL *L*-SP, (5) 1 mM H₂O₂ and 20 μg/mL *L*-SP. Red, caspase-3; blue, 4',6-diamidino-2-phenylindole (DAPI) for nuclei. Scale bars, 50 μm.

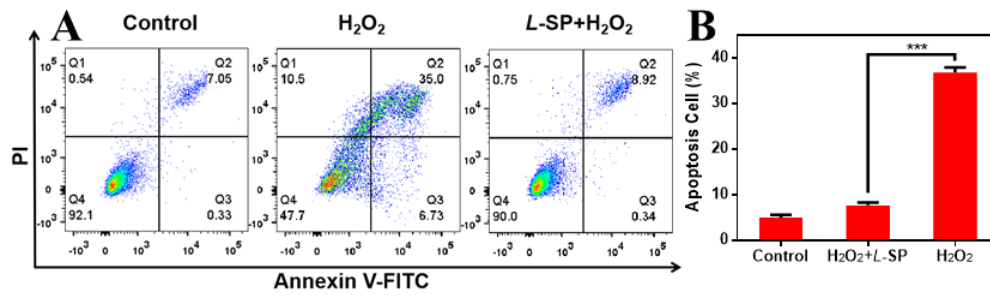


Figure S23. (A) Flow cytometry scatter plot representing apoptosis assay based on annexin V-fluorescein isothiocyanate (Annexin V-FITC)/propidium iodide (PI) staining MN9D cells after different treatments. (B) Population of apoptosis cells summarized from flow cytometry analysis. Data are presented as mean \pm s. d. ($n = 5$).

*** $p < 0.001$.

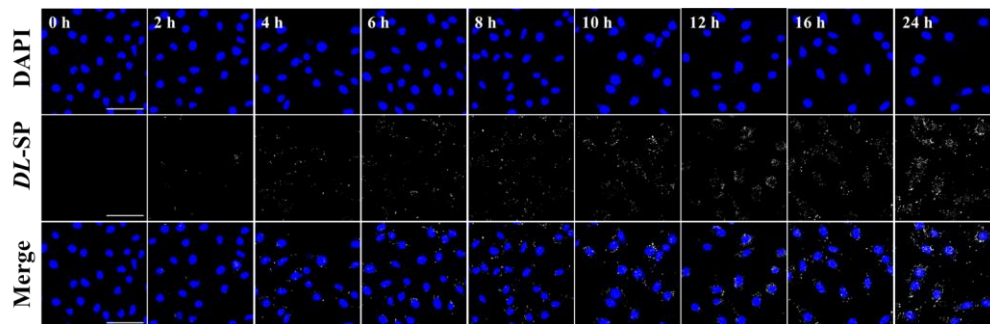


Figure S24. The two-photon luminescence (TPL) images of MN9D cells incubated with the *DL-SP* (10 $\mu\text{g}/\text{mL}$) for different times and washed three times with DPBS.

Scale bars, 40 μm .

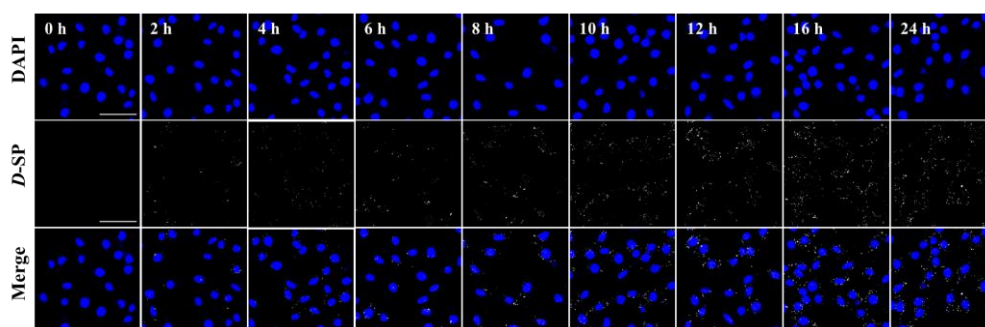


Figure S25. The two-photon luminescence (TPL) images of MN9D cells incubated with the *D*-SP (10 µg/mL) for different times and washed three times with DPBS.

Scale bars, 40 µm.

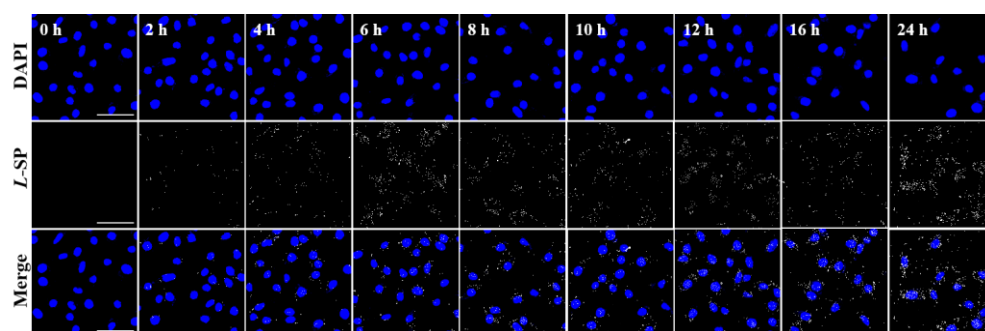


Figure S26. The two-photon luminescence (TPL) images of MN9D cells incubated with the *L*-SP (10 µg/mL) for different times and washed three times with DPBS.

Scale bars, 40 µm.

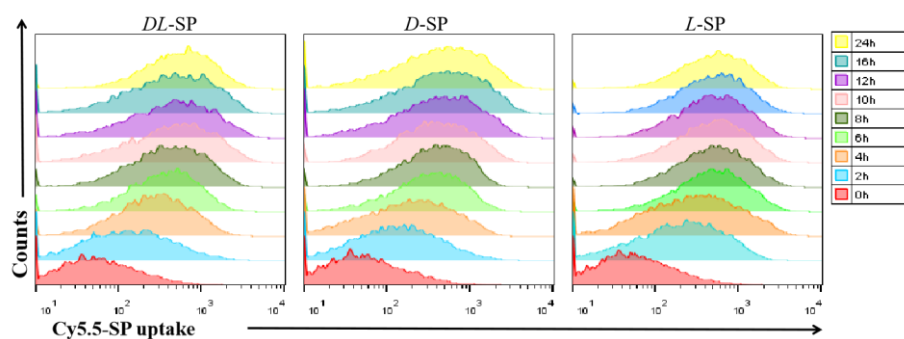


Figure S27. The images of MN9D cells incubated with the *DL*-, *D*-, *L*-SP (10 µg/mL) for different times and washed three times with DPBS from flow cytometry analysis.

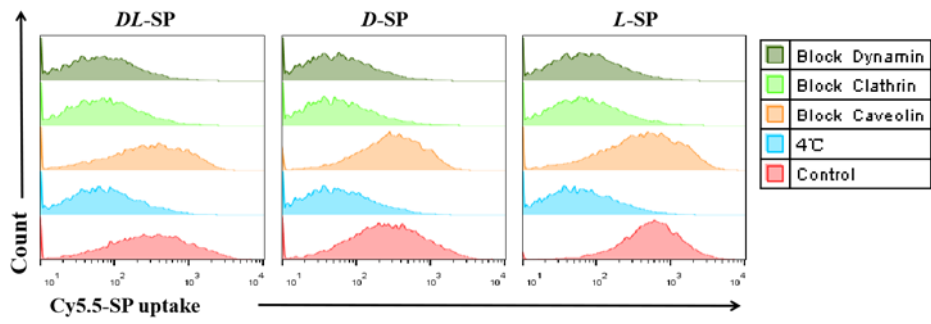


Figure S28. Detection of the amounts of the Cy5.5-SP in MN9D cells by flow cytometry with different treatments.

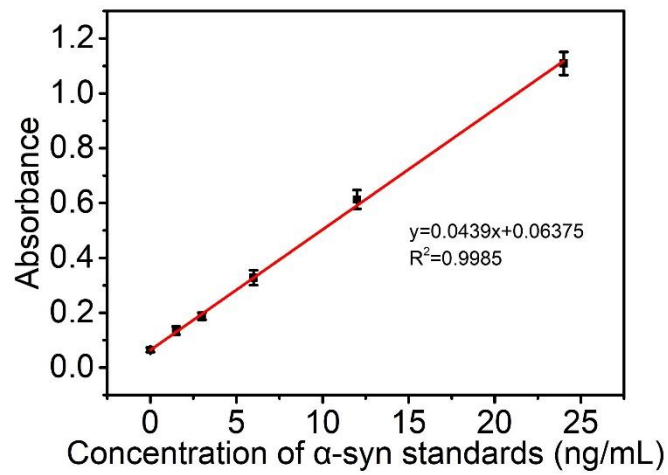


Figure S29. The calibration curve for α -Syn concentration and absorption value.

Data are presented as mean \pm s. d. (n = 5).

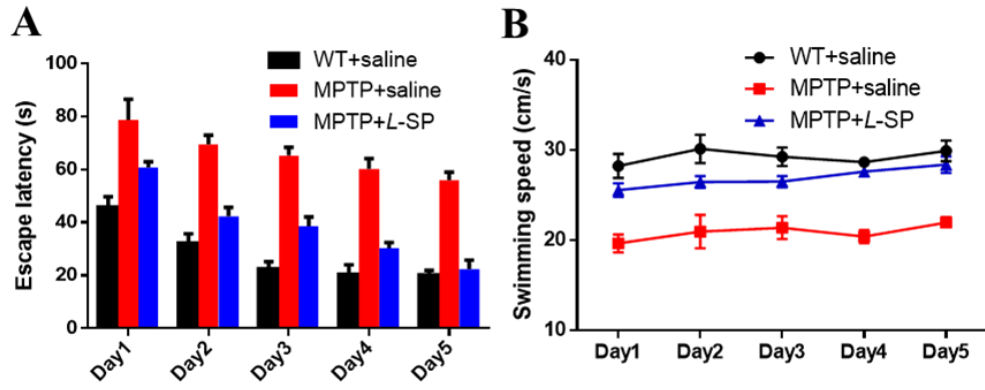


Figure S30. (A) Latency for escape to platform in the training phase. (B) swimming speed in the training phase. Data are presented as mean \pm s. d. (n = 5).

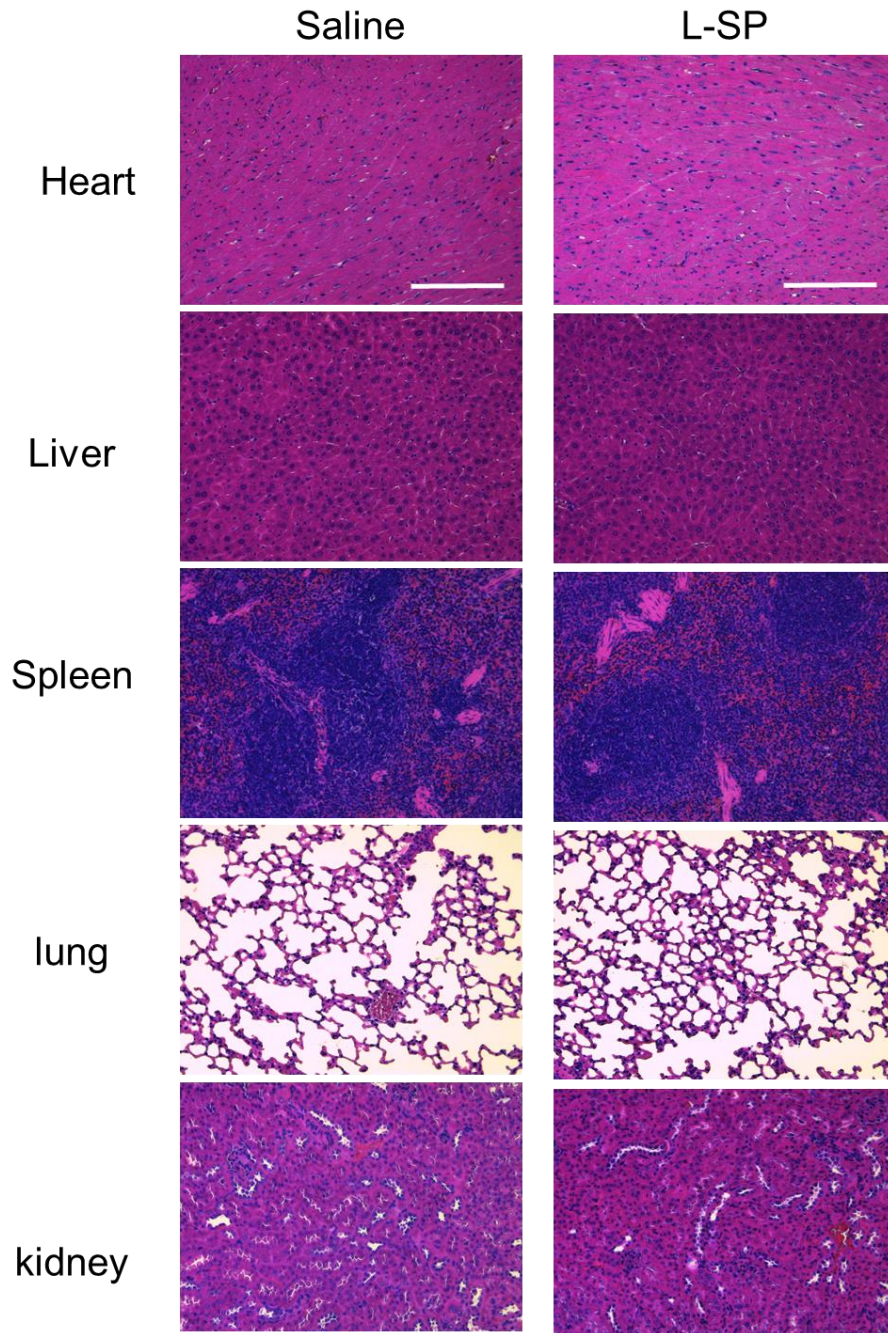


Figure S31. Hematoxylin and Eosin (H&E) stained different organs (heart, liver, kidney, spleen, and lung) after *L-SP* treatments ($n=5$). Scale bars are 100 μm .

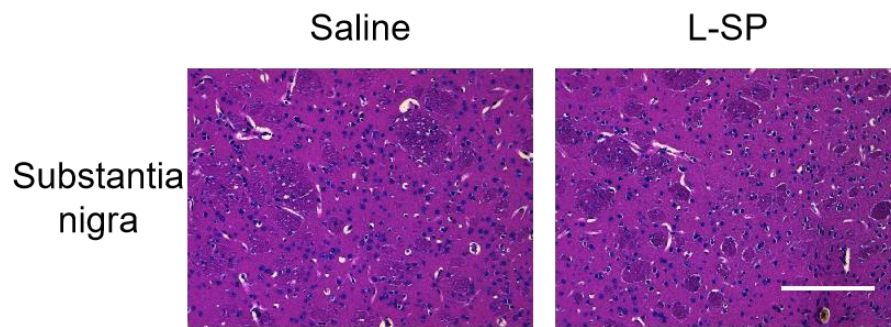


Figure S32. Hematoxylin and Eosin (H&E) stained the substantia nigra after *L*-SP treatments ($n=5$). Scale bars are 100 μm .

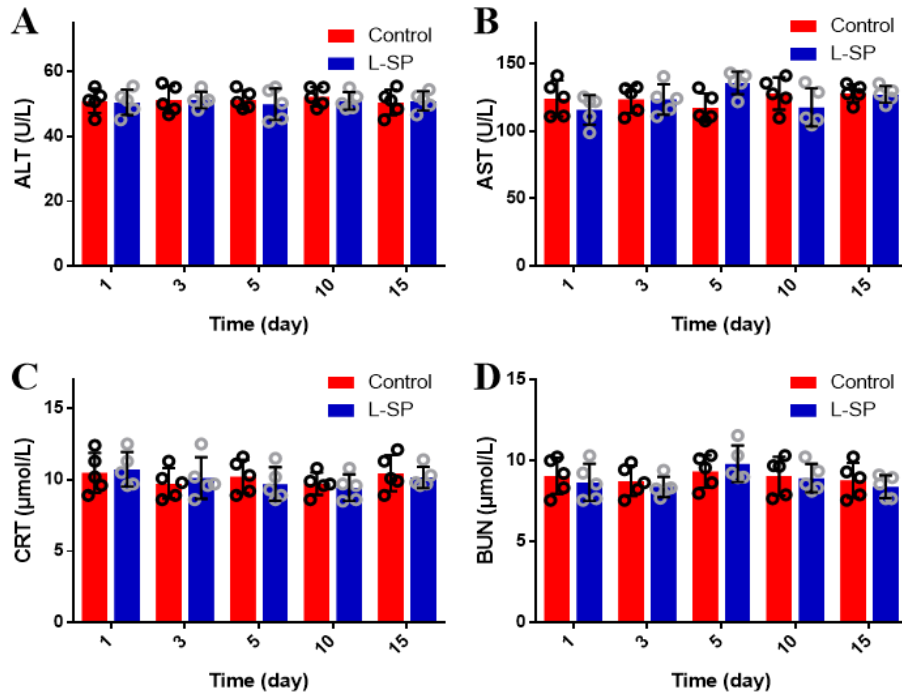


Figure S33. Biochemical assay in the serum of mice ($n=5$).